AIAA JOURNAL
Vol. 47, No. 9, September 2009

Monitoring Impact Events Using a System-Identification Method

Jonghyun Park,* Sungwon Ha,† and Fu-Kuo Chang‡
Stanford University, Stanford, California 94305

DOI: 10.2514/1.34895

An inverse method based on a system-identification technique for identifying impact events on a complex structure with built-in sensors is presented. The method using the transfer functions in the system-identification technique identifies the location and force time history of an impact event on a structure without the need of constructing a full-scale accurate structural model or of acquiring excessive training data on the structure, such as neural-network techniques. The system transfer functions for the entire structure are constructed by two sequential procedures: 1) limited impact tests at selected points to establish the system transfer functions from the selected points to a sensor on the structure and 2) an interpolation function approach based on a linear finite element to approximate the system transfer functions from a point inside four neighboring selected points to the sensor. Comprehensive tests with various impact situations verified the accuracy of load and position predictions by the proposed method.

Nomenclature

A	=	state-space system matrix
$\hat{A}$	=	inverse system matrix
a, b	=	transfer function coefficients
B	=	state-space system vector
$\hat{B}$	=	inverse system vector
C	=	observation matrix
$\hat{C}$	=	inverse observation matrix
D	=	direct throughput matrix
$\hat{D}$	=	inverse direct throughput matrix
$E(\theta)$	=	least-squares error functional
$F(x, y)$	=	input force vector at a point (x, y)
F_i	=	input force vector at the ith node
$F_{(\xi,\eta)}$	=	interpolated input force vector at a point (ξ, η)
f	=	input force signal
H	=	transfer function polynomial matrix
$\hat{H}$	=	inverse transfer function polynomial matrix
h	=	impulse response function
P	=	power
R_s^2	=	multiple correlation coefficient corresponding to sensor output s
S	=	output signal vector
s	=	sensor signal
$\hat{s}$	=	estimated sensor signal
$\boldsymbol{x}$	=	state-space vector
$\hat{\varepsilon}$	=	prediction error
θ	=	adjustable parameter vector
$\hat{\theta}$	=	optimal parameter vector
ϕ	=	interpolation function
φ	=	regression vector

1. Introduction

STRUCTURES can encounter impacts from a variety of sources over their lifetime. Accidental impact can be a serious concern to structural integrity. Especially for composite structures, damage due to impact events may not be visible to surface inspection but still can cause significant loss of structural integrity [1,2]. Therefore, special techniques and equipment are required to inspect this kind of damage, such as x-ray, radiography, or ultrasonic scan, all of which are costly, labor-intensive, and time-consuming for a large structure. A system that automatically detects and reports impact events would make inspections more efficient by localizing the inspection area only for significant impact loading cases.

For impact identification research based on local sensor measurements, there are two basic approaches: model-based techniques [3–15] and neural networks [16–20]. Model-based techniques are based on mathematical models, which must be able to accurately describe the dynamic behavior of structures, including stress wave propagation. In practice, real structures are complicated in configuration and their mechanical properties and boundary conditions may not be known. However, most impact identification studies that have been performed focused primarily on simple structures that are either flat in configuration or have constant properties and simple boundary conditions. However, in practical implementation, the techniques developed from those simple structures cannot be applied directly to practical structures. Seydel and Chang [12,13] identified the location and the history of an impact force applied to stiffened composite panels. They modeled a stiffened panel as an equivalent flat plate with varying properties. By doing so, the governing equation could be derived from the equilibrium equation for a plate. However, for complicated structures, it is still not easy to obtain a mathematical model, such as analytical-model-based approaches or the finite element method. Even if the model can simulate the structural response well, it is difficult to get a simple inverse formulation to reconstruct input force from sensor output. Instead of obtaining an inverse formulation, input forces were constructed by minimizing the difference between the measured response and the calculated response [10–13], which was accomplished by an iterative process. In spite of extensive studies and achievements, the model-based approaches are usually time/labor-consuming. In most cases, these traditional modeling approaches are intractable, and even impossible, for complex structures.

Neural networks calculate outputs through interconnected parallel elements that are adjusted, or trained, so that a particular input leads to a specific target output. However, because these techniques are trained with a specific input, they could lead to a huge error when the pattern of input is different from that of the trained data set, which is very common for different impactors. Only a single impactor was considered for training in all neural-network research [16–20]. They are therefore not practical for use, because the actual type and mass of the impactor may not be known in advance. To confidently use these non-model-based techniques, it is expected that enormous training data must be generated for any practical applications, which is very

Received 1 October 2007; revision received 14 January 2009; accepted for publication 25 April 2009. Copyright © 2009 by the American Institute of Aeronautics and Astronautics, Inc. All rights reserved. Copies of this paper may be made for personal or internal use, on condition that the copier pay the $10.00 per-copy fee to the Copyright Clearance Center, Inc., 222 Rosewood Drive, Danvers, MA 01923; include the code 0001-1452/09 and $10.00 in correspondence with the CCC.

*Structures and Composites Laboratory, Department of Aeronautics and Astronautics; amedio@stanford.edu.

†Research Assistant, Structures and Composites Laboratory, Department of Aeronautics and Astronautics; swhastan@gmail.com.

‡Professor, Structures and Composites Laboratory, Department of Aeronautics and Astronautics; fkchang@stanford.edu. Member AIAA (Corresponding Author).

impractical. In this paper, we propose a new approach for monitoring impact events using a system-identification technique to establish a system model. The system model is constructed in terms of transfer functions on the basis of the relation between input and output. The system model can be applicable to various configurations of structures and can handle various types of impact objects. Also, because it provides a simple inverse formulation to reconstruct input force, the entire impact identification procedure is much simpler and faster than the model-based technique. This research included theoretical development and experimental verification. First, a theoretical basis was found to determine unknown impacts from sensor measurements using a system-identification technique. The technique was verified and evaluated by various experiments.

II. Approach

A. Impact Identification Procedure

An overview of the impact identification approach is shown in Fig. 1. The sensor signals excited from an impact loading are recorded and used to reconstruct forces and to estimate the impact location. For the force reconstruction, the system model was constructed experimentally from impact tests using a system-identification technique. In this research, a distributed piezoelectric sensor array was used to measure the response of a structure due to impact loading.

B. System Model

To obtain a general solution, a system-identification technique was proposed in this study to construct a system model through experimental tests. The system model provides a simple formulation for the inverse procedure to reconstruct forces from output signals. However, traditionally, the approach based on an analytical model is difficult to apply for real structures, and hence it is difficult to obtain an inverse formulation for reconstructing impact force. The neural-network approach is limited to specific impactors that were used to train the system and is hence not practical, because the actual impactor is unknown in reality.

The proposed system model is a mathematical description of the dynamic relationship between the input and output of the structure system, which enables us to calculate the structural response from an impact. In the identification process, realistic and efficient modeling plays a key role. In this research, the system model was constructed in terms of transfer functions from experimental impact tests.

Figure 2 illustrates the basic approach of the constructing the system model for the entire structure based on the transfer function method. First, a transfer function is calculated on the basis of the relation between input force and output sensor signal. In this case, one transfer function represents the relation of a selected point in a structure with respect to a sensor at a specific location (Fig. 2a). Second, a set of transfer functions could be generated for numerous selected points in the structure with respect to a particular sensor. It was assumed that these selected points to generate these transfer functions are physically close enough so that the transfer functions would vary bilinearly from one point to next neighboring points. As a result, the transfer functions at any points in the structure could be constructed through interpolation of four neighboring known

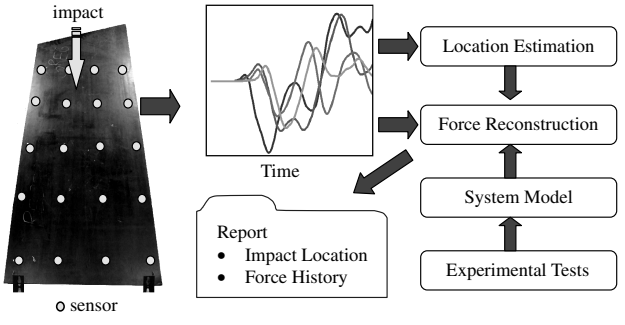

Fig. 1 Overview of impact identification scheme.

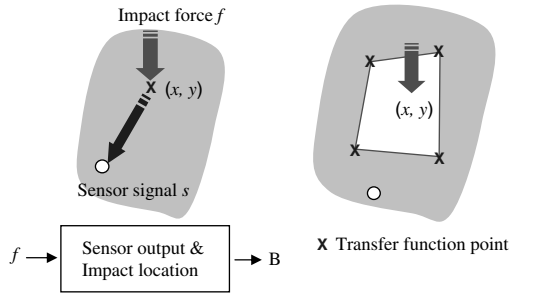

a) A transfer function Bat a specific location (x,y)

b) Four grid points with transfer functions

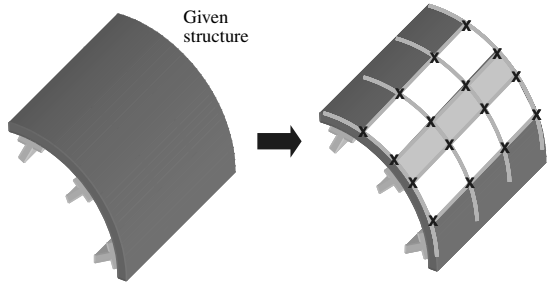

c) Structure covering with grid nodes where transfer functions are developed

Fig. 2 Approach for modeling based on transfer functions.

transfer functions, similar to the finite element interpolation technique (Fig. 2b). Finally, as an impact happens in the area, the impact force could then be constructed from a set of transfer functions in the neighborhood of the impact location, and the details are discussed in Sec. IV.

Accordingly, for a given structure, the entire surface is divided into multiple grids. At each grid node, transfer functions were determined with respect to a particular sensor through training, and so the entire surface can be considered as an assembly of smaller areas confined to the grid nodes (Fig. 2c). Once this assembly process is complete, the system is ready for identifying impact load at any location in the structure.

In this proposed approach, there is no need to construct a mathematical or analytical model for the entire structure in a single operation. Instead, the primary focus is to select a large enough number of grid nodes in training so that the transfer functions could be determined adequately anywhere in the structure for any given impact. Through this approach, the difficulty in constructing an accurate mathematical model for a real structure is removed, and the training sets will be much smaller than that of the neural-network methods because of the use of the transfer functions combined with finite element interpolation technique, which will be discussed in detail in the following.

III. Transfer Function

A. Impulse Response Formulation

Consider an impact for which a force f is applied to a structure at the location (x, y) (Fig. 3). The response s is measured from a sensor at a specific point of the structure.

The response of a structure subjected to an impact force can often be considered to be linearly dependent on the impact force. This linear dependency can be applied when the structure deformation can be considered to be linearly elastic during the impact process and when the deformation of the structure is small enough to neglect geometric nonlinearity. In such cases, the response $s(k)$ can be related to the impact force $f(k)$ by a linear convolution as

$$s(k) = \sum_{i=0}^{k} h(i) f(k-i), \qquad k = 1, 2, 3, \ldots \tag{1}$$

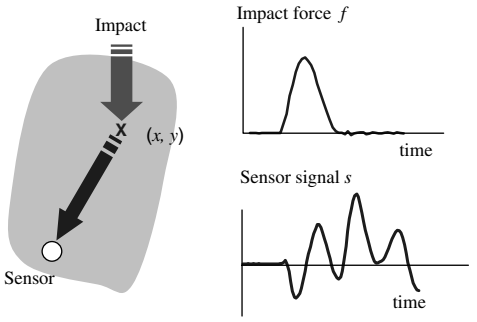

Fig. 3 Impact on a structure.

where $s(k)$ is a sequence of output sensor signal and $f(k)$ is a sequence of input force signals. In Eq. (1), h is the impulse response function of the linear system and the system is assumed to have zero initial conditions. The impulse response function represents the response of the system to unit force pulses and thus it depends on the dynamic properties of the structure.

Consider a structural system of multiple degrees of freedom represented by the discrete-time state-space equation

$$x(k+1) = Ax(k) + Bf(k), \qquad s(k) = Cx(k) + Df(k) \tag{2}$$

where A is a state-space system matrix, B is a state-space system vector, C is a observation matrix, and D is a direct throughput matrix. Assuming zero initial conditions, the system given in Eq. (2) can be stepped forward in time to express the impulse response formulation given by Eq. (1), where $h(i)$ has the form

$$h(0) = D, \qquad h(i) = CA^{i-1}B, \qquad i = 1, 2, \ldots \tag{3}$$

Equation (1) can be expressed in the matrix convolution equation given by

$$S = HF_{(x,y)} \tag{4}$$

where

$$S = [\, s(0) \quad s(1) \quad \cdots \quad s(N-1) \,]^T$$

$$F_{(x,y)} = [\, f(0) \quad f(1) \quad \cdots \quad f(N-1) \,]^T$$

$$H = \begin{bmatrix} h(0) & 0 & \cdots & \cdots & 0 \\ h(1) & h(0) & 0 & \cdots & \vdots \\ h(2) & h(1) & \ddots & 0 & \vdots \\ \vdots & \vdots & \ddots & \ddots & 0 \\ h(N-1) & h(N-2) & \cdots & h(1) & h(0) \end{bmatrix} \tag{5}$$

H is a transfer function polynomial matrix and it relates the input force $F_{(x,y)}$ at (x, y) and a specific sensor signal S. The sensor signal S can be simulated by the simple convolution of $F_{(x,y)}$ and H. In this research, the components of H were obtained from experimental tests using a system-identification technique.

B. System Identification

The goal of system identification is to obtain a mathematical relation that reliably predicts the behavior of outputs using input and output data gathered from the test. Noticeable attention has been given to development of modeling techniques via system identification based on experimental approaches [21–23]. This approach would catch the fundamental dynamic characteristics of the structure and avoid tangled mathematical or physical models. For flexible structures, the system-identification modeling based on the autoregressive with exogenous (ARX) technique has been shown promising results in various applications [21–23]. Accordingly, the ARX technique was chosen in this study to develop the structural model from the sensor data.

1. *Structural Model*

For small displacements, the input/output model of a structure can be reasonably represented by a linear finite difference model [24]. The form of this ARX model is shown in Eq. (6) [24]:

$$s(k) = a_1 s(k-1) + a_2 s(k-2) + \cdots + a_n s(k-n) + b_1 f(k-1) + b_2 f(k-2) + \cdots + b_m f(k-m)$$

or

$$s(k) = \sum_{i=1}^{n} a_i s(k-i) + \sum_{j=1}^{m} b_j f(k-j) \tag{6}$$

It is the task of the system-identification technique to produce estimates of a_i and b_j. From the measurement $(s(k), f(k))$, $\varphi(k)$ is introduced as Eq. (7):

$$\varphi(k) = [s(k-1), \ldots, s(k-n), f(k-1), \ldots, f(k-m)]^T \tag{7}$$

and the adjustable parameters are collected in a vector, as shown in Eq. (8):

$$\theta = [a_1, \ldots, a_n, b_1, \ldots, b_m]^T \tag{8}$$

The model-based prediction for the output at sequence k is

$$\hat{s}(k) = \varphi(k)^T \theta \tag{9}$$

This is referred to as linear regression in statistics, and the vector $\varphi(k)$ is known as the regression vector. The least-squares error functional is

$$E(\theta) = \frac{1}{N} \sum_{k=1}^{N} (\hat{s}(k) - s(k))^2 \tag{10}$$

By minimizing $E(\theta)$, the optimal value of the parameter vector is

$$\hat{\theta} = \left(\sum_{k=1}^{N} \varphi(k) \varphi(k)^T \right)^{-1} \sum_{k=1}^{N} \varphi(k) s(k) \tag{11}$$

This is known as the least-squares estimate.

From a given set of experimental data, a set of modeled data was calculated. These modeled data were compared with the experimental data and a model structure was determined in which the predicted output $\hat{s}$ matched well with the recorded output s. The impulse response function can be expressed from the state-space representation [25], which can be obtained by a canonical realization [26] from a_i and b_j calculated from Eq. (11). So the following is a realization of Eq. (1),

$$x(k+1) = Ax(k) + Bf(k), \qquad s(k) = Cx(k) \tag{12}$$

and the matrices are expressed as follows:

$$A = \begin{bmatrix} a_1 & a_2 & \cdots & a_{n-1} & a_n \\ 1 & 0 & \cdots & 0 & 0 \\ \vdots & 1 & \cdots & 0 & 0 \\ \vdots & \vdots & \ddots & \vdots & \vdots \\ 0 & 0 & \cdots & 1 & 0 \end{bmatrix}, \qquad B = \begin{bmatrix} 1 \\ 0 \\ 0 \\ \vdots \\ 0 \end{bmatrix}$$

$$C = [\, b_1 \quad b_2 \quad \cdots \quad b_m \,] \tag{13}$$

From Eqs. (3), (5), and (13), all the components of the transfer function H can be expressed in terms of system parameters a_i and b_j.

2. *Choice of Model Order*

A significant difficulty in parametric identification of ARX models is that to construct the regression vector $\varphi(k)$, one needs to know the degree n of the denominator. In fact, an incorrect choice for n will generally lead to difficulties.

First, selecting too large of a value for n is called over-parameterization, and it leads to the transfer matrix being close to singular. Second, selecting too small of a value for n will lead to mismatch between the measured data and the model, and error or residuals will be large.

To adjust parameterized models to data systematically, some criterion must be used. The most common one is to minimize the prediction error. It is possible to evaluate the prediction in Eq. (9) at sequence k if the prediction error

$$\varepsilon(k,\theta) = s(k) - \varphi(k)^T\theta \tag{14}$$

is computed. From Eq. (14), the error is associated with the adjustable value θ and is called the prediction error corresponding to θ.

$$\hat{\varepsilon}(k) = \varepsilon(k,\hat{\theta}) \tag{15}$$

Equation (15) defines the *residuals* associated with the optimal parameter vector $\hat{\theta}$. Often, it is desired to investigate how well the predicted output $\hat{s}(k)$ explains the actual output. According to [24], the ratio

$$R_s^2 = 1 - \frac{\sum_{k=1}^{N}\hat{\varepsilon}^2(k)}{\sum_{k=1}^{N}s^2(k)} \tag{16}$$

measures the proportion of the total variation of s that is explained by the regression. It is called the *multiple correlation coefficient*.

To select the appropriate model order, the following simple model structure selection is used:

1) Start with the smallest model possible.

2) Increase the model order until the multiple correlation coefficient R_s^2 is close enough to 1 so that the model matches well with the measured data.

3) If R_s^2 is close enough to 1 and increasing the model order does not sufficiently increase the value of R_s^2, select the model with the smallest order.

C. Inverse Formulation

To reconstruct force history from given sensor data due to impact loading, the inverse formulation of a system is constructed. Using the transfer function described in Sec. III.B, the force history can be calculated from an inverse procedure.

Equation (2) can be manipulated to interchange the input and output [25], yielding the inverse structural system equation:

$$x(k+1) = \hat{A}x(k) + \hat{B}s(k), \qquad f(k) = \hat{C}x(k) + \hat{D}s(k) \tag{17}$$

where the inverse state-space system matrix, state-space system vector, observation matrix, and direct throughput matrix are defined as

$$\hat{A} = [A - BD^+C], \qquad \hat{B} = BD^+, \qquad \hat{C} = -D^+C$$
$$\hat{D} = D^+ = (D^TD)^{-1}D^T \tag{18}$$

For a stable inverse system, an impulse response sequence can be expressed similarly to the forward system:

$$f(k) = \sum_{i=0}^{k}\hat{h}(i)s(k-i) \tag{19}$$

where $\hat{h}(i)$, an impulse response of the inverse system, is given by

$$\hat{h}(0) = \hat{D}, \qquad \hat{h}(i) = \hat{C}\hat{A}^{i-1}\hat{B}, \qquad i = 1,2,\ldots \tag{20}$$

To obtain the inverse structure system equation, Eq. (12) must be stepped forward in time. The new forward system is

$$x(k+1) = Ax(k) + Bf(k)$$
$$s(k+1) = Cx(k+1) + CBf(k) \tag{21}$$

The inverse system associated with Eq. (21) is noncausal. That is, the estimate of the input force at time k is now a function of the response at future times, $k+1$ through $k+l$. In general, the first $l-1$ impulse response functions in Eq. (1) are zero: that is, $CB = CAB\cdots CA^{l-2}B = 0$. Based on the assumption of zero initial conditions, the inverse model can be constructed:

$$f(k) = \sum_{i=0}^{k}\hat{h}(i)s(k+l-i) \tag{22}$$

where the impulse response function of the inverse system are given by

$$\hat{h}(0) = \hat{D}, \qquad \hat{h}(i) = \hat{C}\hat{A}^{i-1}\hat{B}, \qquad i = 1,2,\ldots \tag{23}$$

and now

$$\hat{A} = [A - B(CA^{l-1}B)^+(CA^l)], \qquad \hat{B} = B(CA^{l-1}B)^+$$
$$\hat{C} = -(CA^{l-1}B)^+(CA^l), \qquad \hat{D} = (CA^{l-1}B)^+ \tag{24}$$

Equation (22) can be expressed in the matrix convolution equation given by

$$F_{(x,y)} = \hat{H}S \tag{25}$$

where

$$F_{(x,y)} = [\,f(0) \quad f(1) \quad \cdots \quad f(N-l-1)\,]^T$$
$$S = [\,s(l) \quad s(l+1) \quad \cdots \quad s(N-1)\,]^T$$
$$\hat{H} = \begin{bmatrix} \hat{h}(0) & 0 & \cdots & \cdots & 0 \\ \hat{h}(1) & \hat{h}(0) & 0 & \cdots & \vdots \\ \hat{h}(2) & \hat{h}(1) & \ddots & 0 & \vdots \\ \vdots & \vdots & \ddots & \ddots & 0 \\ \hat{h}(N-l-1) & \hat{h}(N-l-2) & \cdots & \hat{h}(1) & \hat{h}(0) \end{bmatrix} \tag{26}$$

$\hat{H}$ is the inverse transfer matrix, and all components are calculated from the system parameters a_i and b_j from Eq. (13). By using Eq. (25), the desired input force can be computed by the simple convolution of the sensor output signals and the inverse transfer matrix $\hat{H}$.

IV. Force Construction for General Locations

In Eq. (25), a transfer function represents the relation between a single point in a structure and a specific sensor response. To cover the whole structure, a discrete number of $\hat{H}$ at preselected grid nodes are obtained over the structure from experimental tests. The impact force at general locations other than at the grid points can be constructed in terms of the impact forces obtained at a certain set of discrete $\hat{H}$ points. As discussed in the following paragraphs, this can be achieved using a shape-function approach that is typically used in the finite element methods.

A. Interpolation Function Approach

Consider a set of $\hat{H}$ obtained at 4 grid points, as shown in Fig. 4, with 4 nodes numbered 1 through 4. The ith node has physical coordinates (x, y), and the area bounded by 4 nodes is considered as an element of a set of transfer functions. For this, we can associate a regular element of the same topology, for which the edges have a nondimensional length. The corresponding nodes in this parametric space have coordinates (ξ, η). The physical and parametric coordinates are linked by the basis functions. For two-dimensional bilinear interpolation, these functions are shown in Eq. (27):

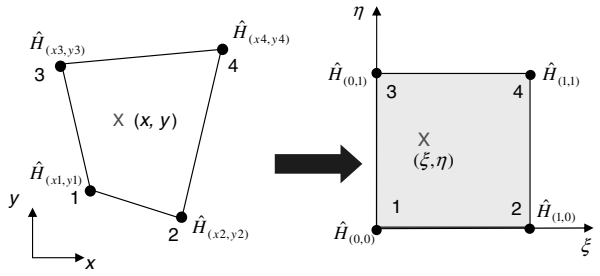

Fig. 4 Mapping a general point.

$$\phi_1(\xi,\eta) = (1-\xi)(1-\eta), \qquad \phi_2(\xi,\eta) = \xi(1-\eta)$$
$$\phi_3(\xi,\eta) = (1-\xi)\eta, \qquad \phi_4(\xi,\eta) = \xi\eta \tag{27}$$

This same interpolation of position is used to interpolate impact forces associated with each node. If a sensor signal S is obtained due to an impact at a point (ξ, η), the force at the ith node F_i can be constructed using Eq. (25):

$$F_1 = \hat{H}_{(0,0)}S, \qquad F_2 = \hat{H}_{(1,0)}S, \qquad F_3 = \hat{H}_{(0,1)}S$$
$$F_4 = \hat{H}_{(1,1)}S \tag{28}$$

Then the interpolated F at a point (ξ, η) is found from

$$F_{(\xi,\eta)} = \sum_{i=1}^{4} \phi_i F_i \tag{29}$$

Once an area is defined by a set of transfer function points, any impact force in the area can be constructed from Eq. (29). Using this approach, a whole structure can be modeled with a small number of transfer functions, which eliminates the need for numerous impact tests to determine transfer functions for the structure.

B. Spacing for Transfer Functions

The accuracy of the force reconstruction in Eq. (29) is dependent on the spacing of points (the grid nodes) for the transfer functions. Generally, the accuracy decreases as the spacing increases. To see the effect of the spacing points, an example impact test was performed. Sensors were mounted on a composite structure with uniform thickness and the sensor spacing was 1.22×1.22 m (Fig. 5).

First, transfer functions were obtained at 4 points with a specific spacing and then additional impact tests were performed on evaluation points inside of the area bounded by 4 points. The force at the evaluation point was constructed using Eq. (29). The difference between the force constructed and the forced recorded was checked for different spacings. The error is defined in Eq. (30) as the ratio of difference in amplitudes (as shown in Fig. 6):

$$\text{error}\,(\%) = \frac{|\text{amplitude recorded} - \text{amplitude reconstructed}|}{\text{amplitude reconstructed}} \cdot 100 \tag{30}$$

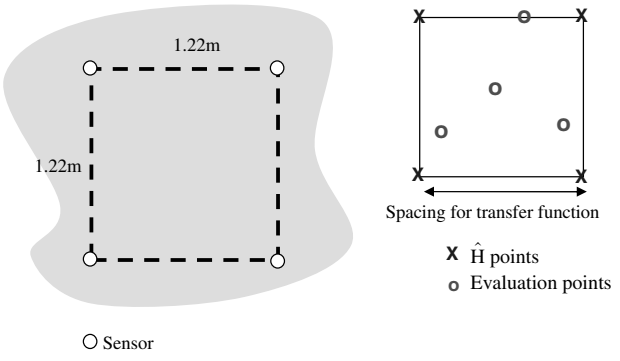

Fig. 5 Impact test for spacing effect.

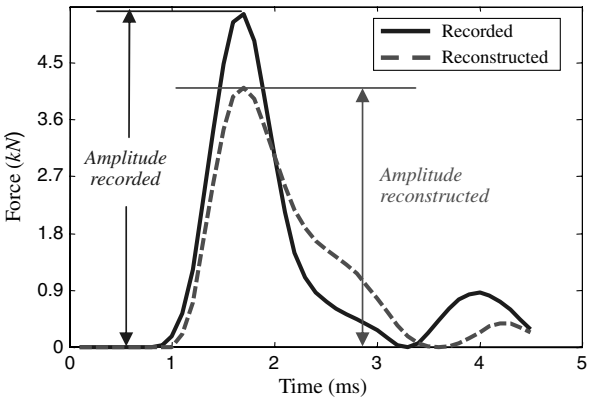

Fig. 6 Amplitude difference between forces recorded and reconstructed.

The results in Fig. 7 show that the error decreases as the spacing decreases. In this case, the error was less then 10% for 0.3 m spacing and about 20% error was estimated for 45 in. spacing.

Through this simple test, the spacing for transfer function points can be determined for the required accuracy.

V. Estimating Impact Location

To determine the impact location, an initial estimate was made using a power distribution method to be discussed in Sec. V.A. Then the location was updated by minimizing the differences in the forces reconstructed from multiple sensors, as will be discussed in Sec. V.B.

A. Initial Estimation of Impact Location

In most previous studies, time-of-flight information is used to find a location estimate. Figure 8 illustrates several methods for finding

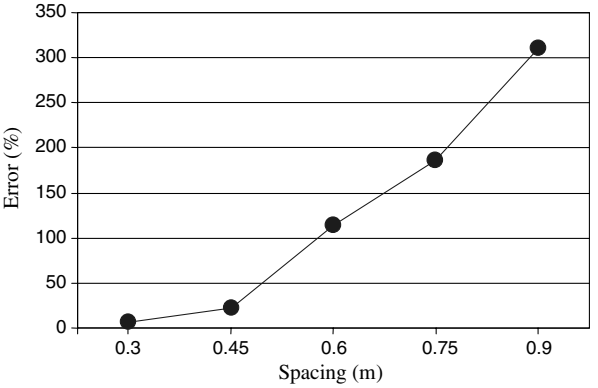

Fig. 7 Force reconstruction errors vs transfer function spacing.

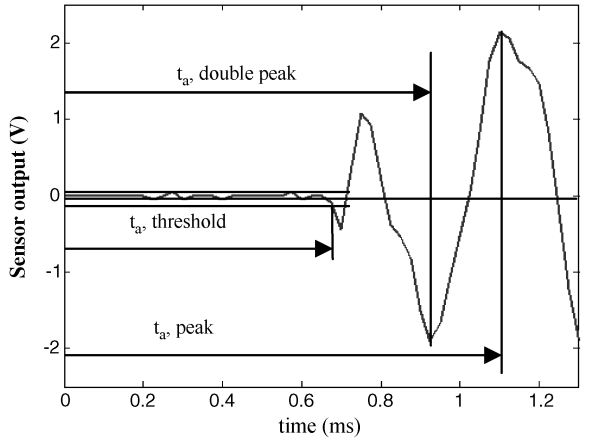

Fig. 8 Illustration of arrival-time definition.

the time of arrival of the impact wave: threshold [5], peak-signal [25], and double-peak methods [12].

The threshold method picks the time when the signal first exceeds an assumed noise level, and the peak-signal method picks the time of the maximum sensor signal. Seydel and Chang [12] proposed determining arrival time by selecting the minimum before the maximum for each signal. This threshold method is vulnerable to the uncertainty of the assumed noise level and the peaks are not always as clear as those shown in Fig. 8 for complicated structures. For this reason, we proposed a new method for estimating an impact location: impact location was estimated by calculating the centroid of power distribution over a structure from sensor signals due to impact loading. When a structure has abundant sensors for monitoring impact events, the power distribution due to impact loading can provide a good estimation for the impact location. First, the method used to determine root-mean-square (rms) power is discussed. Next, the approach used to find a location estimate from the power is discussed.

For a given a signal $s(t)$, the energy of the signal is shown in Fig. 9. The energy of the signal is the shaded area of squared signal. Power is a time average of energy, and signal power is defined for a given time window as follows:

$$\text{power} = P = \frac{1}{t_f - t_0}\int_{t_0}^{t_f} |s(t)|^2 \mathrm{d}t \tag{31}$$

where t_0 = initial time and t_f = final time.

The rms power of a signal is defined as follows:

$$P_{\text{rms}} = \sqrt{P} = \sqrt{\frac{1}{t_f - t_0}\int_{t_0}^{t_f} |s(t)|^2 \mathrm{d}t} \tag{32}$$

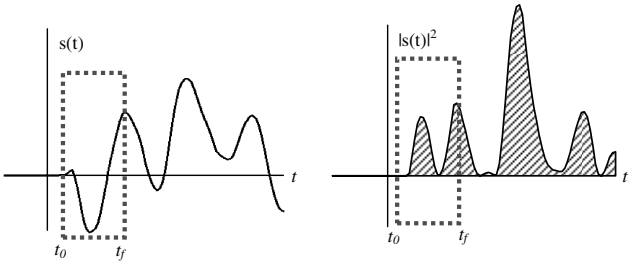

Fig. 9 Energy of a signal.

In this research, rms power was used to obtain the power distribution. Once the power for all sensors was calculated in a given time window, the power distribution was found over the structure. Figure 10 shows the method used to obtain the power distribution.

Once impact occurred, the signals due to the impact loading were recorded from the sensors distributed over the structure. From Eq. (32), the power of each signal was calculated in a given time window. Then the power value was calculated at each sensor location in the structure, and, by interpolation, a smooth power distribution was obtained so that the interpolating surface satisfied the biharmonic equation and therefore had minimum curvature. Once the smooth power distribution was found, the power was expressed in terms of x and y coordinates:

$$P_{\text{rms}i} = P_{\text{rms}i}(x_i, y_i), \qquad i = 1, 2, 3, \ldots \tag{33}$$

From the power distribution found in Eq. (33), the impact location was estimated in terms of the centroid of the power. For the 2-D case, the centroid was calculated as follows:

$$\bar{x}_c = \frac{\sum P_{\text{rms}i} x_i}{\sum P_{\text{rms}i}}, \qquad \bar{y}_c = \frac{\sum P_{\text{rms}i} y_i}{\sum P_{\text{rms}i}} \tag{34}$$

where $\bar{x}_c$ = center of the x axis, and $\bar{y}_c$ = center of the y axis.

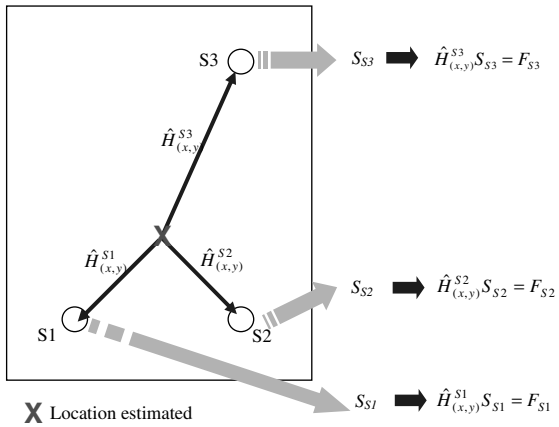

Fig. 11 Force reconstructed from the location estimated.

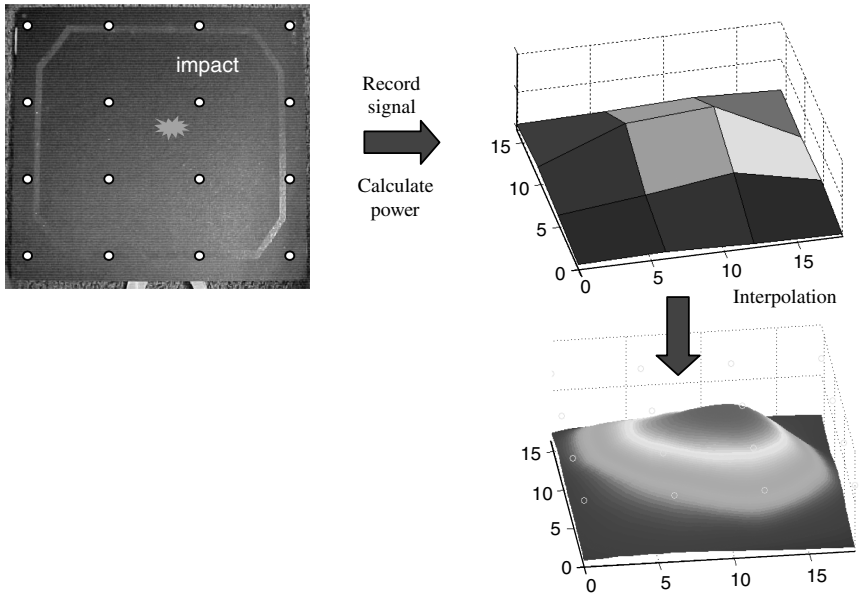

Fig. 10 Power distributions over a structure.

B. Update Location Using Multiple Sensors

From an initial estimate, the impact location was updated by minimizing a cost function J [Eq. (35)]. Figure 11 shows an example of reconstructing force from an estimated location with 3 sensors $S1$, $S2$, and $S3$. For each sensor, the transfer functions are calculated. ($\hat{H}^{S1}_{(x,y)}$ for sensor $S1$, $\hat{H}^{S2}_{(x,y)}$ for sensor $S2$, and $\hat{H}^{S3}_{(x,y)}$ for sensor $S3$). Because of external impact loading, sensor signals are recorded for each sensor: S_{S1}, S_{S2}, and S_{S3}. From an estimated location, forces are reconstructed for each sensor using Eq. (25) and they are F_{S1}, F_{S2}, and F_{S3}.

The cost function J is given as follows:

$$J = (F_{S1} - F_{S2})^2 + (F_{S2} - F_{S3})^2 + (F_{S3} - F_{S1})^2 \qquad (35)$$

The location-update procedure searches for the location at which the cost function J is minimized.

To help visualize the search for the impact location, a contour surface of the cost function J was constructed for an example impact, as shown in Fig. 12. The structure is the same composite structure shown previously and the sensor spacing is 1.22×1.22 m. The J was calculated from Eq. (35) using the signals of sensors $S1$, $S2$, and $S3$. The resulting contour of the cost function J is shown in Fig. 13 for the isolated area ABCD. The contour shows one global minimum and the location-update procedure finds this minimum point of the cost function.

VI. Experimental Tests

A. Specimens

For the experiment, two stiffened panels were used. Figure 14 shows their geometries. Specimen 1 was 0.38 by 0.38 m with an I-beam stiffener running the length of the panel. Specimen 2 was manufactured from T800H/3900-2 graphite epoxy by The Boeing Company. The panel size is roughly 1.57 by 0.53 m and has three parallel I-beam stiffeners. The sensor spacing was 0.165 by 0.254 m. The piezoceramic sensors and associated wiring were mounted on the panel surface using the SMART Layer™ technique developed by Lin et al. [27], which was fabricated using a printed circuit technique.

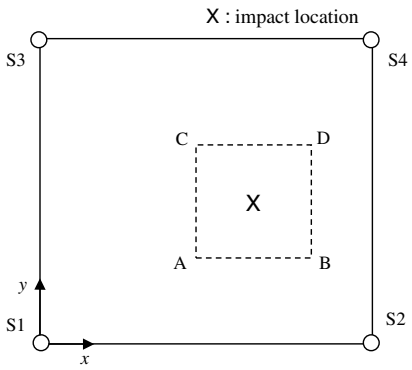

Fig. 12 An example impact.

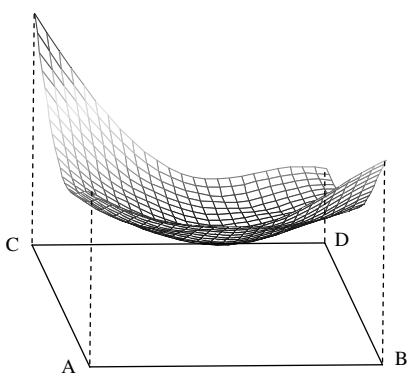

Fig. 13 Contour of the cost function J.

B. Experimental Setup

The panels were impacted by a handheld instrumented hammer manufactured by PCB Piezotronics. Both the sensor data created by the impact and the force data from the hammer were recorded using a data acquisition system manufactured by National Instruments. Samples were taken at 40 kHz and all data were in the range of ± 10 V.

The stiffened panels were used for evaluation of the impact identification technique and evaluation of various types of impactors.

C. Impact Tests

To obtain transfer functions, experimental impact tests were performed on specimens 1 and 2. They were used for experimental model verification and evaluation of location estimation. Experimental impacts were made with random force magnitude at each location. Transfer functions were calculated at each impact point using hammer signals and sensor signals from the tests. Impact locations are shown in Fig. 15. Because of the symmetry of the structure, this transfer function set could cover the whole panel, including the boundaries.

D. Verification of Transfer Function

1. Choice of Model Order

To select the model order (i.e., the order of the model polynomial n), we investigated the multiple correlation coefficient R^2_s, defined in Eq. (16).

To illustrate model-order selection, an example impact is shown in Fig. 16. An impact test was performed on the stiffener area of specimen 1 by using the handheld instrumented hammer, and the hammer signal and the sensor signal were recorded. Figures 16b and 16c show the signals from the hammer and sensor 1.

From the given hammer signal $f(k)$ and the sensor signal $s(k)$, the system model was constructed. To choose the order of the model, n was increased from 2, and the results of the simulation were obtained for n up to 8. For each n, m in Eq. (6) is selected to maximize the value of R^2_s. In Fig. 17, the simulation results are presented for the cases

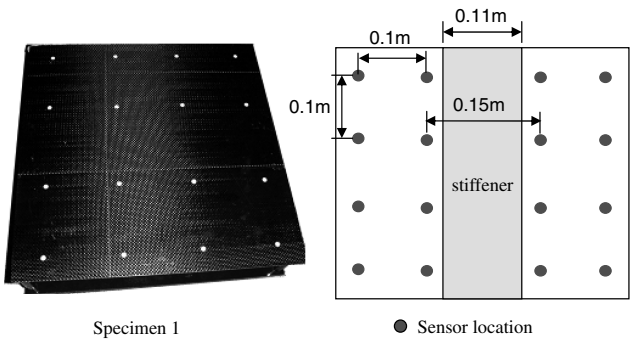

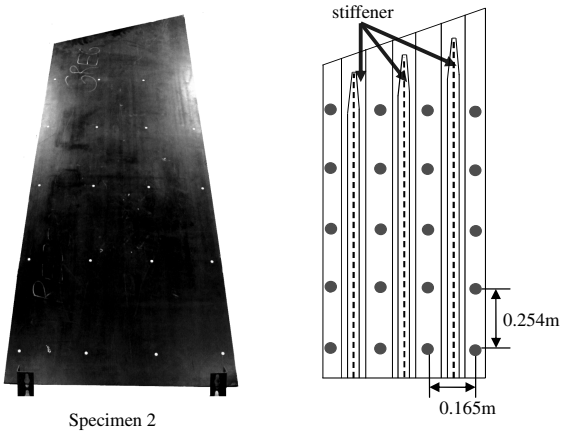

Fig. 14 Geometry of two stiffened panels (specimens 1 and 2) and sensor locations.

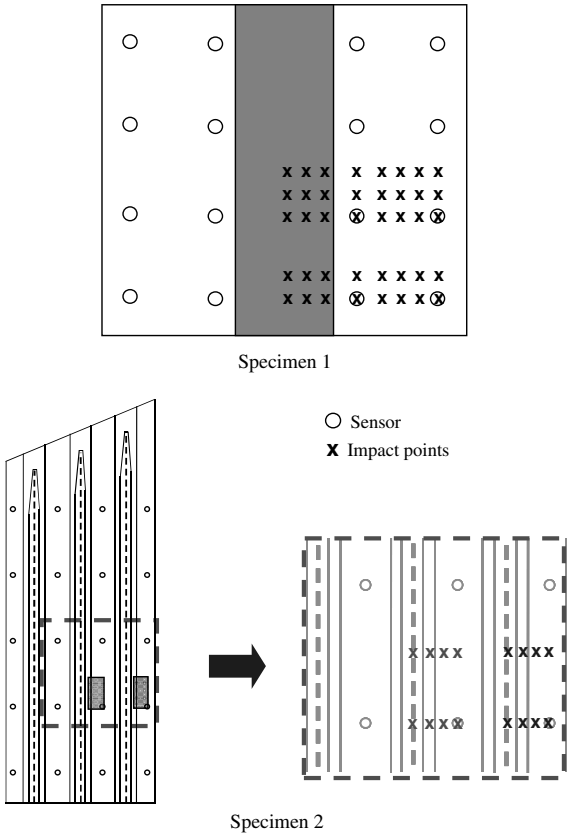

Fig. 15 Experimental impact locations for obtaining transfer functions.

$n = 2$, 3, 4, and 5. As the order of the system was increased, the simulated results matched more closely with the measured data and there was little change between $n = 4$ and 5.

To see the effect of the system order, the multiple correlation coefficient R_s^2 was calculated, and the results are shown in the in Fig. 18. The knee point in the figure occurs with the configuration $n = 4$, and there is practically no advantage in increasing the model order beyond this point. Accordingly, the order of the transfer function was set to 4 for this case.

2. *Validation of Transfer Function with Different Impact Objects*

In the procedure of calculating transfer functions, the transfer functions were verified by simulating sensor signals from given input signals. This was done on a new set of data. For the validation of the transfer function, a new input sequence was created with different impact hammer and was sent through the transfer function. The simulated outputs were compared with sensor signals recorded and this gave an indication of model accuracy. Figure 19 shows the simulation results with different impactors. First, a transfer function was constructed using the impact hammer with a copper tip (Fig. 19a). Using the same transfer function, the simulated results

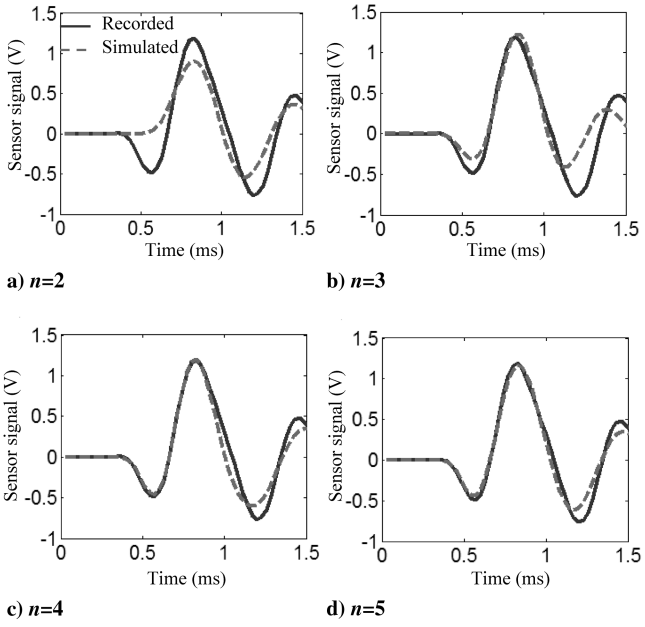

Fig. 17 Simulation results with different n.

were compared with recorded sensor signals using a different hammer tip. For both plastic and rubber tips, the simulating signals matched well with the recorded signals. Thus, the transfer function was considered to be capable of reproducing the response of the real system.

VII. Results

To illustrate the proposed process, only results for specimen 2 are presented here. The results of specimen 1 can be found in [28].

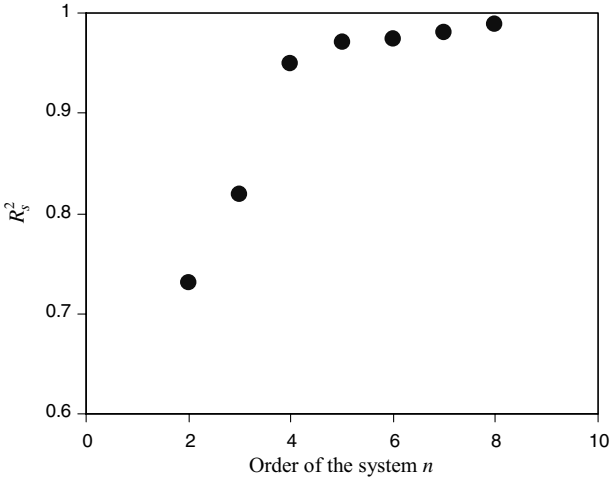

Fig. 18 Multiple correlation coefficients as a function of model order n.

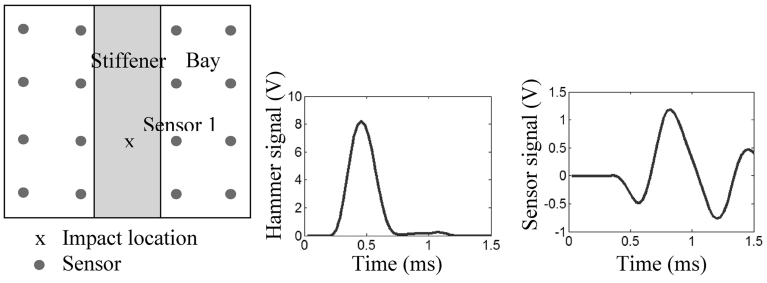

Fig. 16 Example of input/output signal of an impact.

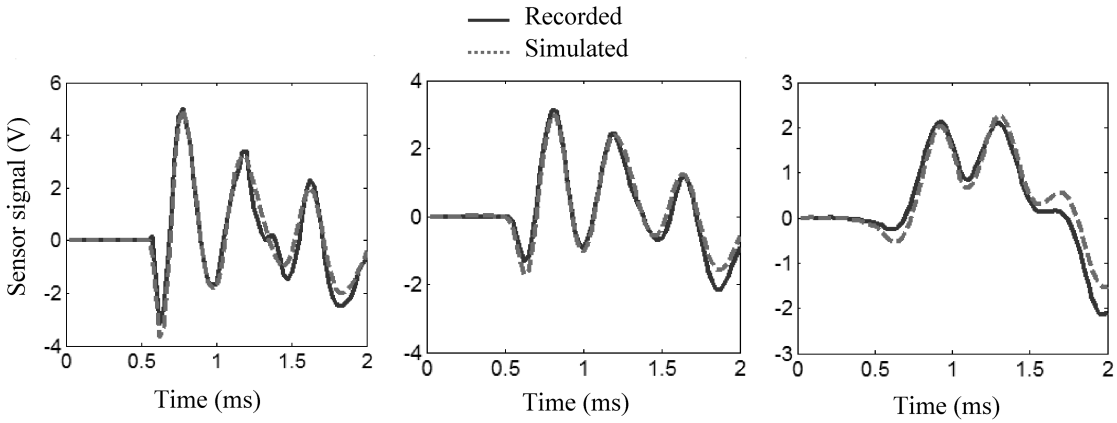

a) Copper tip **b) Plastic tip** **c) Rubber tip**

Fig. 19 Simulation results for different impactors.

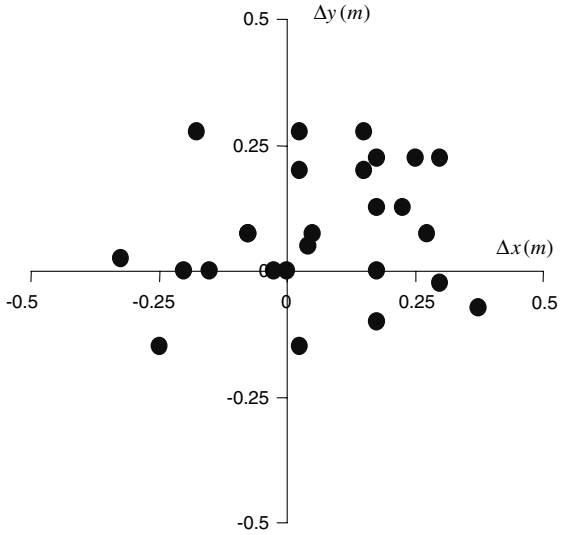

Fig. 20 Location estimation errors for the stiffened panel.

A. Location Estimation

For the stiffened panel, experimental impact tests were made at random locations, including the stiffener area and bay area. Location error is defined as the distance from the actual impact location to the calculated location, where the y direction is the direction of the stiffener:

$$\text{location error} = \sqrt{(\Delta x^2 + \Delta y^2)} \tag{36}$$

where $\Delta x = x_{\text{impact}} - x_{\text{calc}}$ and $\Delta y = y_{\text{impact}} - y_{\text{calc}}$. The location estimation error is shown in Fig. 20, and the average error for the location was 0.02 m.

B. Force Reconstruction

An example of force reconstruction is shown in Fig. 21. The force was reconstructed from sensor signals and transfer functions obtained from 16 points shown in Fig. 15. The results of force reconstruction were well-matched with the hammer signals recorded in the stiffened area (Fig. 21b), bay area (Fig. 21c), and even near the edge (Fig. 21d).

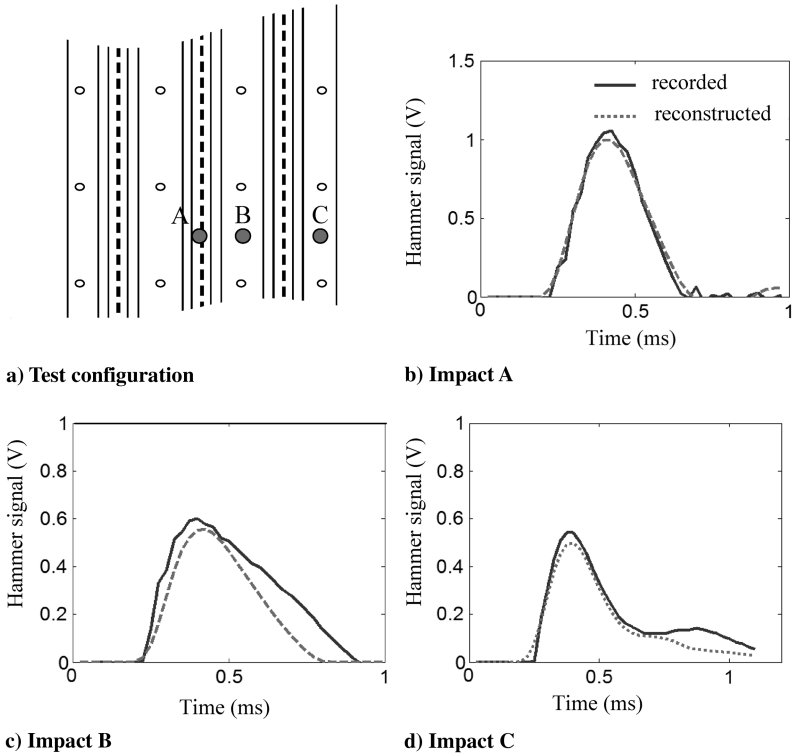

a) Test configuration **b) Impact A**

c) Impact B **d) Impact C**

Fig. 21 Force reconstructions for the stiffened panel.

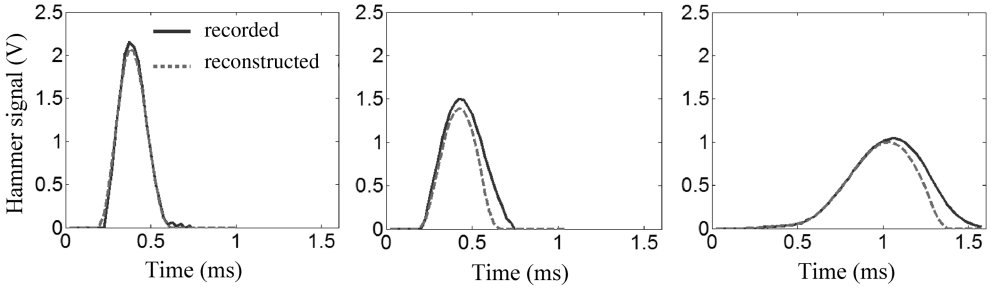

a) Copper tip **b) Plastic tip** **c) Rubber tip**

Fig. 22 Force reconstructions for hammer tip materials.

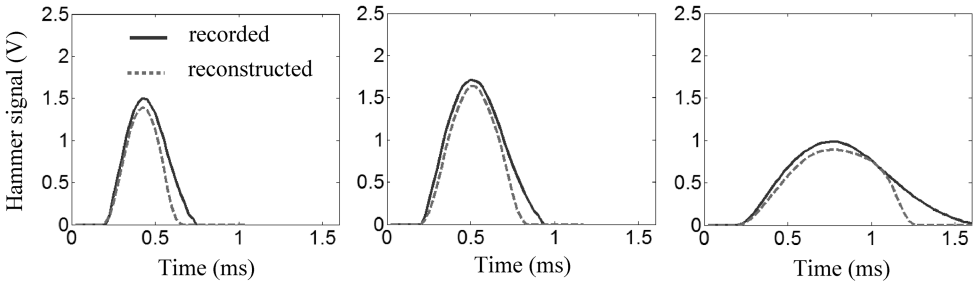

a) Mass 0.161 kg **b) Mass 0.239 kg** **c) Mass 0.615 kg**

Fig. 23 Force reconstructions for hammer masses with a plastic tip.

C. Various Types of Impact Objects

Additional experiments were performed to verify the force reconstruction methodology for various impactors. First, a transfer function was obtained from an impact test using an impact hammer. The hammer tip was made of copper and the mass of impactor was 0.161 kg. Using the transfer function obtained from the hammer, force reconstruction was performed for various impact tests with different impactors.

Figure 22 shows the results of force reconstruction with different material tips. With the given transfer function, the reconstruction results matched well with the hammer signals recorded in terms of both amplitude and time duration. Figure 23 presents the force reconstruction for different masses. For increasing mass, the increasing time duration in the reconstruction matched well with the experimental results.

VIII. Conclusions

With limited training data, an impact identification technique was proposed to create an inverse of a system model of a structure for predicting the impact location and force history of the structure upon impact by a foreign object in a real environment. The proposed technique significantly reduces the amount of training data required for current non-model-based impact detection techniques and also avoids the construction of an accurate mathematical model, which is required for model-based impact detection techniques but may not be possible in practice. This approach showed good success at finding impact location and force history for impact loadings with various impactors, which had different masses and material types, on stiffened panels.

It is worth noting, however, that the accuracy of the proposed technique relies on two essential assumptions:

1) The transfer functions within four neighboring training grid nodes can be accurately interpolated from the four transfer functions at the nodes. This implies that a structure with a complex geometry and sudden changes in mechanical properties requires finer grids with more training data sets.

2) The responses of sensors are duplicable at the similar locations within the structure. This may impose a challenge for large structures if each sensor was installed individually. Data may still need to be collected for similar regions at different locations in the structure.

References

[1] Miller, A. G., Lovell, D. T., and Seferis, J. C., "The Evolution of an Aerospace Material: Influence of Design, Manufacturing and In-Service Performance," *Composite Structures*, Vol. 27, Nos. 1–2, 1994, pp. 193–206.
doi:10.1016/0263-8223(94)90080-9

[2] Bartelds G., "Aircraft Structural Health Monitoring, Prospects for Smart Solutions from a European Viewpoint Structural Health Monitoring. Current Status and Perspectives," *Proceedings of the International Workshop on Structural Health Monitoring*, DEStech, Lancaster, PA, 1997, pp. 293–300.

[3] Okafor, A. C., Chandrashenkhara, K., and Jiang, Y. P., "Location of Impact in Composite Plates Using Waveform-Based Acoustic Emission and Gaussian Cross-Correlation Techniques," *Proceedings of SPIE—The International Society for Optical Engineering*, Vol. 2718, 1996, pp. 291–302.
doi:10.1117/12.240895

[4] Michel, L. D., Labeerrere, M., Gafsi, R., Malki, A. R., and Lecoy, P., "Impact Detection and Vibration Sensing for Material Composite Structures by Integrated Optic Fibre Sensors," *Proceedings of SPIE—The International Society for Optical Engineering*, Vol. 2718, 1996, pp. 291–302.
doi:10.1117/12.240895

[5] Gunther, M. F., Wang, A., Fogg, B. R., Starr, S. E., Murphy, K. A., and Claus, R. O., "Fiber Optic Impact Detection and Location System Embedded in a Composite Material," *Proceedings of SPIE—The International Society for Optical Engineering*, Vol. 1798, 1993, pp. 262–269.
doi:10.1117/12.141322

[6] Doyle, J. F., "Experimentally Determining the Contact Force During the Transverse Impact of an Orthotropic Plate," *Journal of Sound and Vibration*, Vol. 118, No. 3, 1987, pp. 441–448.
doi:10.1016/0022-460X(87)90363-4

[7] Martin, M. T., and Doyle, J. F., "Impact Force Identification from Wave Propagation Responses," *International Journal of Impact Engineering*, Vol. 18, No. 1, 1996, pp. 65–77.
doi:10.1016/0734-743X(95)00022-4

[8] Wu, E., Yeh, J.-C., and Yen, C.-S., "Identification of Impact Forces at Multiple Locations Laminated plates," *AIAA Journal*, Vol. 32, No. 12, 1994, pp. 2433–2439.
doi:10.2514/3.12310

[9] Choi, K., and Chang, F.-K., "Identification of Impact Force and Location Using Distributed Sensors," *AIAA Journal*, Vol. 34, No. 1, 1996, pp. 136–142.
doi:10.2514/3.13033

[10] Tracy, M., and Chang, F.-K., "Identifying Impacts in Composite Plates with Piezoelectric Strain Sensors. Part 1: Theory," *Journal of Intelligent Material Systems and Structures*, Vol. 9, No. 11, 1998, pp. 920–928.

[11] Tracy, M., and Chang, F.-K., "Identifying Impacts in Composite Plates with Piezoelectric Strain Sensors. Park 2: Experiments," *Journal of Intelligent Material Systems and Structures*, Vol. 9, No. 11, 1998, pp. 929–937.

[12] Seydel, R., and Chang, F. K., "Impact Identification of Stiffened Composite Panels. 1: System Development," *Smart Materials and Structures*, Vol. 10, No. 2, 2001, pp. 354–369. doi:10.1088/0964-1726/10/2/323

[13] Seydel, R., and Chang, F. K., "Impact identification of Stiffened Composite Panels. 2: Implementation Studies," *Smart Materials and Structures*, Vol. 10, No. 2, 2001, pp. 370–379. doi:10.1088/0964-1726/10/2/324

[14] Park, C. Y., Lee, J. H., Kim, I.-G., and Lee, Y.-S., "Low Velocity Impact Monitoring for Composite Sandwich Panels Using PVDF Sensor," *Proceedings of the 2nd European Workshop on Structural Health Monitoring*, DEStech, Lancaster, PA, 2004, pp. 423–430.

[15] Hu, N., and Fukunaga, H., "Health Monitoring of Composite Structures Based on Impact Force Identification," *Proceedings of the 2nd European Workshop on Structural Health Monitoring*, DEStech, Lancaster, PA, 2004, pp. 415–422.

[16] Chandrashekara, K., Okafor, A. C., and Jiang, Y. P., "Estimation of Contact Force on Composite Plates Using Impact Induced Strain and Neural Network," *Proceedings of SPIE—The International Society for Optical Engineering*, Vol. 2718, 1996, pp. 320–330. doi:10.1117/12.240871

[17] Akhavan, F., Watkins, S. E., and Chandrashekara, K., "Recovery of Impact Contact Forces of Composite Plates Using Fiber Optic Sensors and Neural Networks," *Proceedings of SPIE—The International Society for Optical Engineering*, Vol. 2839, 1996, pp. 277–288. doi:10.1117/12.255363

[18] Jones, R. T., Sirkis, J. S., and Friebele, E. J., "Detection of Impact Location and Magnitude for Isotropic Plates Using Neural Networks," *Journal of Intelligent Material Systems and Structures*, Vol. 7, No. 1, 1997, pp. 90–99.

[19] Worden, K., and Staszewski, W. J., "Impact Location and Quantification on a Composite Panel Using Neural Networks and a Genetic Algorithm," *Strain*, Vol. 36, No. 2, 2000, pp. 61–70. doi:10.1111/j.1475-1305.2000.tb01175.x

[20] Haywood, J., Staszewski, W. J., and Worden, K., "Impact Location in Composite Structures Using Smart Sensor Technology and Neural Networks," *Proceedings of the 3rd International Workshop on Structural Health Monitoring*, DEStech, Lancaster, PA, 2001, pp. 1466–1475.

[21] Manning, W., Plummer, A. R., and Levelsley, M. C., "Vibration Control of a Flexible Beam with Integrated Actuators and Sensors," *Smart Materials and Structures*, Vol. 9, No. 6, 2000, pp. 932–939. doi:10.1088/0964-1726/9/6/325

[22] Lee, Y., and Elliott, S. J., "Active Position Control of a Flexible Smart Beam Using Internal Model Control," *Journal of Sound and Vibration*, Vol. 242, No. 5, 2001, pp. 767–791. doi:10.1006/jsvi.2000.3379

[23] Bai, M. R., and Lin, G. M., "The Development of a DSP-Based Active Small Amplitude Vibration Control System for Flexible Beams by Using the LQG Algorithm and Intelligent Materials," *Journal of Sound and Vibration*, Vol. 198, No. 4, 1996, pp. 411–427.

[24] Juang, J.-N., *Applied System Identification*, Prentice–Hall, Upper Saddle River, NJ, 1994.

[25] Kammer, D. C., "Estimation of Structural Response Using Remote Sensor Locations," *Journal of Guidance, Control, and Dynamics*, Vol. 20, No. 3, 1997, pp. 501–508. doi:10.2514/2.4069

[26] Kailath, T., *Linear Systems*, Prentice–Hall, Upper Saddle River, NJ, 1980.

[27] Lin, M., Kumbar, A., Beard, S., and Qing, X., "Built-In Structural Diagnostic with the SMART Layer™ and SMART Suitcase™," *Smart Materials Bulletin*, Vol. 2001, No. 4, 2001, pp. 7–11. doi:10.1016/S1471-3918(01)80123-4

[28] Park, J., "Monitoring Impact Event Using a System Identification Technique," Ph.D. Dissertation, Dept. of Aeronautics and Astronautics, Stanford Univ., Stanford, CA, 2006.

C. Cesnik
Associate Editor